# NATURAL CONVECTION HEAT TRANSFER WITHIN VERTICALLY ECCENTRIC DOMED SKYLIGHTS CAVITIES

A. Sartipi [1], A. Laouadi [2], D. Naylor [3], R. Dhib [4]

[1] Department of Mechanical and Industrial Engineering, Ryerson University, aSartipi@Ryerson.ca
[2] National Research Council of Canada, Abdelaziz.Laouadi@nrc-cnrc.gc.ca
[3] Department of Mechanical and Industrial Engineering, Ryerson University, dNaylor@Ryerson.ca
[4] Department of Chemical Engineering, Ryerson University, rDhib@Ryerson.ca

## ABSTRACT

Domed skylights are important architectural design elements to deliver daylight and solar heat into buildings and connect building's occupants to outdoor. However, most of building energy simulation programs do not cover such skylights to quantify their energy performance when installed in buildings. This paper presents a numerical study on natural laminar convection within vertically eccentric domed cavities when heated from the exterior surface. Both interior and exterior surfaces are held at uniform temperatures. A commercial CFD package employing the control volume approach is used to solve the laminar convective heat transfer within the cavity. The obtained results showed that the flow is mono-cellular for small and moderate heating intensities as depicted by the Grashof number. For high Grashof numbers, small vortex cells appear within a larger vortex cell at the lower part of the cavity. The multi-cellular flow increases heat transfer. The critical gap spacing that yields the maximum heat transfer was quantified for several dome profiles.

## KEYWORDS

Natural laminar convection; domed cavity; domed skylight, eccentric domed cavity

## NOMENCLATURE

| | |
|---|---|
| $k$ | Fluid thermal conductivity |
| $L_{max}$ | Maximum gap thickness |
| $L_{min}$ | Minimum gap thickness |
| $L$ | Local gap thickness |
| $P$ | Pressure |
| $P^*$ | Dimensionless pressure |
| $q_{cond}$ | Pure conduction heat transfer |
| $q_i$ | Convection heat transfer from interior surface |
| $q_o$ | Convection heat transfer from exterior surface |
| $R_o$ | Outer radius |
| $R_i$ | Inner radius |
| $r$ | Position radius |
| $r^*$ | Dimensionless position radius |
| $T$ | Temperature |
| $T^*$ | Dimensionless temperature |
| $u_r$ | Velocity component in r-direction |
| $u_\theta$ | Velocity component in θ-direction |

*Greek Symbols*

| | |
|---|---|
| $\alpha$ | Fluid thermal diffusivity |
| $\beta$ | Fluid thermal expansion coefficient |
| $\delta_{max}$ | Maximum dimensionless gap thickness($L_{max}/R_o$) |
| $\delta_{min}$ | Minimum dimensionless gap thickness ($L_{min}/R_o$) |
| $\delta$ | Dimensionless local gap thickness ($L/R_o$) |
| $\nu$ | Kinematic viscosity |
| $\theta$ | Position angle |
| $\theta_o$ | Dome truncation angle |
| $\rho$ | Fluid density |
| $\tau$ | Dimensionless time |

*Dimensionless Numbers*

| | |
|---|---|
| Gr | Grashof number, $[g\beta(T_o-T_i)L_{max}^3/\nu^2]$ |
| Nu | Nusselt number, $[h\ L_{max}/k]$ |
| Pr | Prandtl number, $[\nu/\alpha]$ |
| Ra | Rayleigh number ($Ra = Gr.Pr$) |
| Ra* | Modified Rayleigh number, Eq. (15) |

## INTRODUCTION

Domed skylights are commonly used in buildings such as residential, industrial and commercial buildings. They deliver daylight and solar heat into the indoor environment and connect building's occupants to the outdoor environment. If properly designed, domed skylights may reduce the building energy usage for lighting, cooling and heating. Furthermore, current research has shown that daylighting and connection to outdoor have positive effects on occupants' mood and wellbeing. Despite their wide spread use, the thermal performance of domed skylights has not been well understood. Current design tools such as fenestration product rating tools and building energy simulation software do not cover this type of skylights. This paper addresses the natural laminar convective heat transfer in vertically eccentric domed skylight cavities heated from outside. The inside and outside surfaces are held at uniform different temperatures, and the edge surfaces are sealed and adiabatic. The main objectives are to investigate the flow pattern in the cavity, quantify the critical gap spacing that yields the maximum heat transfer, and develop correlations for the convective heat transfer coefficient as a function of the governing parameters.

## MATHEMATICAL FORMULATION

A double-layer domed skylight with the eccentricity of (ε) is the subject of this study. The dome cavity is characterized by its interior and exterior radii ($R_i$, $R_o$), minimum and maximum gap thicknesses ($L_{min}$, $L_{max}$) and truncation angle ($\theta_0$). The interior and exterior domed surfaces are maintained at uniform temperatures $T_i$ and $T_o$, respectively. The edges of the domed cavity are sealed and adiabatic. The cavity is filled with a gaseous fluid. The truncation angle may vary from $0^o$ to $90^o$, covering almost flat horizontal cavities or fully hemispheric cavities. Since the dome is symmetric with respect to the Y-axis (revolution axis), the flow is considered two-dimensional. Figure 1 shows a schematic representation of a double-layer domed cavity.

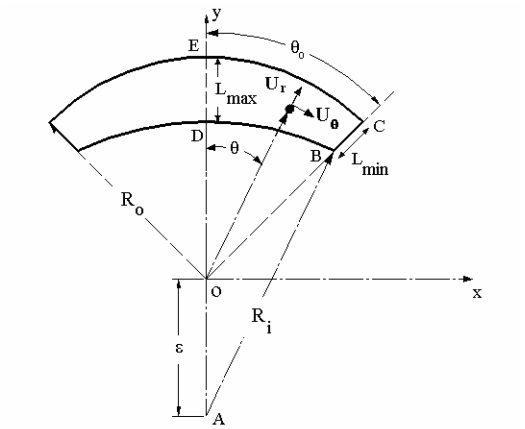


*Figure 1 Schematic description of a double-layer domed cavity*

### Assumptions

The governing equations for mass, momentum and energy transfer balances are written in the spherical co-ordinate system. The following assumptions are made to simplify the governing equations;

- The fluid is incompressible, Newtonian and laminar;
- The physical properties of the fluid are constant, except the density in the body force terms;
- Boussinesq approximation is used for the buoyancy terms; and
- The viscous dissipation is neglected in the energy equation.

### Governing Equations

The simplified governing equations are cast in a dimensionless form using the following dimensionless variables;

$$r^* = \frac{r}{L_{\max}},\ \tau = \frac{t}{\left(L_{\max}^2/\upsilon\right)},\ U_r = \frac{u_r}{\left(\upsilon/L_{\max}\right)},\ U_\theta = \frac{u_\theta}{\left(\upsilon/L_{\max}\right)},\quad (1)$$
$$P^* = \frac{p}{\rho_i\left(\upsilon/L_{\max}\right)^2},\ T^* = \frac{T-T_i}{T_o-T_i}$$

Substituting those dimensionless variables into the governing equations, the resulting transient dimensionless governing equations reduce to:

Continuity:

$$\frac{1}{r^*}\frac{\partial}{\partial r^*}\left(r^{*2}U_r\right)+\frac{1}{\sin\theta}\frac{\partial}{\partial\theta}\left(U_\theta\sin\theta\right)=0 \quad (2)$$

r-momentum:

$$\frac{\partial U_r}{\partial\tau}+U_r\frac{\partial U_r}{\partial r^*}+\frac{U_\theta}{r^*}\frac{\partial U_r}{\partial\theta}-\frac{U_\theta^2}{r^*}=-\frac{\partial P^*}{\partial r^*}-Gr\cdot T^*\cos\theta+ \quad (3)$$
$$\frac{1}{r^{*2}}\frac{\partial^2}{\partial r^{*2}}\left(r^{*2}U_r\right)+\frac{1}{r^{*2}\sin\theta}\frac{\partial}{\partial\theta}\left(\sin\theta\frac{\partial U_r}{\partial\theta}\right)$$

θ-momentum

$$\frac{\partial U_\theta}{\partial\tau}+U_r\frac{\partial U_\theta}{\partial r^*}+\frac{U_\theta}{r^*}\frac{\partial U_\theta}{\partial\theta}+\frac{U_rU_\theta}{r^*}=-\frac{1}{r^*}\frac{\partial P^*}{\partial\theta^*}+Gr\cdot T^*\sin\theta+ \quad (4)$$
$$\frac{1}{r^{*2}}\frac{\partial}{\partial r^*}\left(r^{*2}\frac{\partial U_\theta}{\partial r^*}\right)+\frac{1}{r^{*2}}\frac{\partial}{\partial\theta}\left(\frac{1}{\sin\theta}\frac{\partial}{\partial\theta}\left(U_\theta\sin\theta\right)\right)+\frac{2}{r^{*2}}\frac{\partial U_r}{\partial\theta}$$

Energy:

$$\Pr\left[\frac{\partial T^*}{\partial\tau}+U_r\frac{\partial T^*}{\partial r^*}+\frac{U_\theta}{r^*}\frac{\partial T^*}{\partial\theta}\right]=\frac{1}{r^{*2}}\frac{\partial}{\partial r^*}\left(r^{*2}\frac{\partial T^*}{\partial r^*}\right)+\frac{1}{r^{*2}\sin\theta}\frac{\partial}{\partial\theta}\left(\sin\theta\frac{\partial T^*}{\partial\theta}\right) \quad (5)$$

### Dimensionless Boundary Conditions

The dimensionless governing equations (2) to (5) are subject to the following boundary conditions: the dome ends are sealed and adiabatic; the exterior and interior surfaces are maintained at uniform and constant temperatures and no-slip condition. The dimensionless boundary conditions are as follows:

Edge surface,

$$U_\theta=U_r=0,\ \frac{\partial T^*}{\partial\theta}=0\ \text{at}\ \theta=\theta_0,\ \frac{1}{\delta_{\max}}-\frac{\delta_{\min}}{\delta_{\max}}<r^*<\frac{1}{\delta_{\max}} \quad (6)$$

Symmetry surface,

$$U_\theta=0,\ \frac{\partial T^*}{\partial\theta}=0\ \text{at}\ \theta=0,\ \frac{1}{\delta_{\max}}-1<r^*<\frac{1}{\delta_{\max}} \quad (7)$$

Exterior surface,

$$U_r=U_\theta=0,\ T^*=1\ \text{at}\ r^*=\frac{1}{\delta_{\max}} \quad (8)$$

Interior surface,

$$U_r=U_\theta=0,\ T^*=0\ \text{at}\ r^*=\frac{1}{\delta_{\max}}-\frac{\delta}{\delta_{\max}} \quad (9)$$

with:

$$\frac{1}{\delta_{\max}}=\frac{R_o}{L_{\max}};\ \frac{1}{\delta_{\min}}=\frac{R_o}{L_{\min}};\ \frac{1}{\delta}=\frac{R_o}{L};\ \frac{1}{\delta_{ave}}=\frac{R_o}{L_{ave}} \quad (10)$$

Where $L_{ave} = (L_{max} + L_{min})/2$ and L is the local gap thickness at position angle θ.

At the initial conditions (τ = 0), the fluid is assumed quiescent and, therefore, the heat transfer is by pure

conduction. The dimensionless governing equations and boundary conditions show that the cavity flow is governed by the Grashof number (Gr), Prandtl number (Pr), dimensionless gap spacing ($\delta_{max}$), the ratio of the minimum to maximum gap spacing ($L_{min}/L_{max}$) and truncation angle ($\theta_0$).

## NUMERICAL METHOD

The control volume approach is used to discretize the dimensionless governing equations. A commercial CFD package is used to solve the discretized equations.

The heat transfer problem was investigated for a wide range of geometry and boundary conditions: the Grashof number (Gr) varies from $10^3$ to $10^7$, non-dimensional gap spacing ($\delta_{max}$) varies between 0.008 and 0.5, and three different truncation angles ($\theta_o$) of 30°, 45° and 90°. The ratio of the maximum to minimum gap thickness is fixed to $L_{max}/L_{min} = 2$. For all geometries, different mesh sizes were used to ensure mesh-independent results. A non-uniform grid in the radial direction with finer mesh sizes near the walls was used to account for the temperature and velocity gradients near the interior and exterior surfaces.

The governing equations were solved numerically using the implicit and segregated scheme [4]. A second order upwind scheme is used to discretize the momentum and energy equations (3) to (5). The SIMPLEC algorithm [4] was used for the pressure-velocity coupling and PRESTO algorithm for the pressure correction, which is recommended for buoyancy-driven problems [5].

### Validation of the Numerical Method

For the model validation purposes, the results from the uniform gap thickness model ($L_{min}/L_{max} = 1$) are compared with those obtained by Laouadi and Atif [1], Raithby and Holand [2] and Grag [3] for concentric spheres when heated from inside. Table 1 shows this comparison. The maximum difference between the present model and the other models is less than 1%.

*Table 1. Nusselt number for concentric spheres heated from inside for $\delta_{max} = \delta_{min} = 0.5$*

| RA | Present model | Laouadi and Atif [1] | Grag [3] | Raithby and Hollands [2] |
|---|---|---|---|---|
| 3000 | 1.4180 | 1.420 | 1.4213 | 1.2610 |
| 6300 | 1.7346 | 1.737 | 1.7393 | 1.5180 |
| 10500 | 1.9800 | 1.980 | 1.9848 | 1.7248 |
| 14000 | 2.1283 | 2.127 | 2.1331 | 1.8534 |
| 21000 | 2.3511 | 2.345 | 2.3560 | 2.0511 |
| 42000 | 2.7707 | 2.760 | 2.7761 | 2.4392 |
| 91000 | 3.303 | 3.283 | 3.3110 | 2.9594 |

## EVALUATION OF HEAT TRANSFER

The heat transfer from the interior and exterior surfaces of the domed cavities are evaluated as follow:

$$q_i = -2\pi R_i^2 k \int_0^{\theta_o} \left.\frac{\partial T}{\partial r}\right|_{r=R_i} \sin\theta d\theta \tag{11}$$

$$q_o = -2\pi R_o^2 k \int_0^{\theta_o} \left.\frac{\partial T}{\partial r}\right|_{r=R_o} \sin\theta d\theta \tag{12}$$

For cavities of non-uniform gap thicknesses, the conduction heat transfer is two-dimensional, which has a complicated equation in the spherical co-ordinate system. In this paper for convenience, the Nusselt number is defined for the interior and exterior surfaces as follows:

$$Nu_i = \frac{q_i}{q'_{cond}} = \frac{\frac{(R_i/R_o)^2}{\delta_{max}}\frac{\delta_{ave}}{1-\delta_{ave}}}{1-\cos\theta} \int_0^{\theta_o} \left.\frac{\partial T^*}{\partial r^*}\right|_{r^*=\frac{1}{\delta_{max}}-\frac{\delta}{\delta_{max}}} \sin\theta d\theta \tag{13}$$

$$Nu_o = \frac{q_o}{q'_{cond}} = \frac{\frac{1}{\delta_{max}}\left(\frac{\delta_{ave}}{1-\delta_{ave}}\right)}{1-\cos\theta} \int_0^{\theta_o} \left.\frac{\partial T^*}{\partial r^*}\right|_{r^*=\frac{1}{\delta_{max}}} \sin\theta \cdot d\theta \tag{14}$$

Where $q'_{cond}$ is the conduction heat flux of a concentric cavity with an average gap thickness equal to $L_{ave} = (L_{max} + L_{min})/2$.

Under the steady state conditions, the heat transfer and Nusselt number at the interior surface are equal to the exterior surface ($q_i = q_o = q$ & $Nu_i = Nu_o = Nu$).

## RESULTS AND DISCUSSION

The numerical results are presented when the exterior surface is hotter than the interior one and air (Pr = 0.72) is used in the cavity gap. Small, moderate and large gap thicknesses are the subject of this study. The flow reaches the steady state conditions for small and moderate Grashof numbers, independently of the truncation angles and gap thickness. For the Grashof number around $2.5x10^6$, small unstable vortex cells form inside a big cell, which causes small oscillations in the Nusselt number. Figure 2 shows typical oscillations for a truncation angle of 30°, $\delta_{max}$ =0.008 and Gr = $7.5x10^6$. It is found that in most of the times these oscillations are periodic. Under such periodic transient conditions, the Nusselt number is averaged over two or three oscillation periods.

Figure 3 shows the streamlines and isotherms for small, moderate and large gap cavities for two different truncation angles of 90° and 45°. The Grashof number is fixed at $5x10^4$. For all cases, the cavity flow reaches the steady-state conditions with only one vortex cell. As the Grashof number increases, one or more small cells form inside a big cell. Figure 4 shows the comparison of streamlines and isotherms for three different gap thicknesses and two truncation angles of 90° and 45°. For large cavity gap thicknesses ($\delta_{max} > 0.2$), the flow reaches the steady-state conditions with one small cell

inside a big cell for both 90° and 45° truncation angles. However, for moderate and small gap thicknesses, small multi-cells appear inside the big vortex cell.

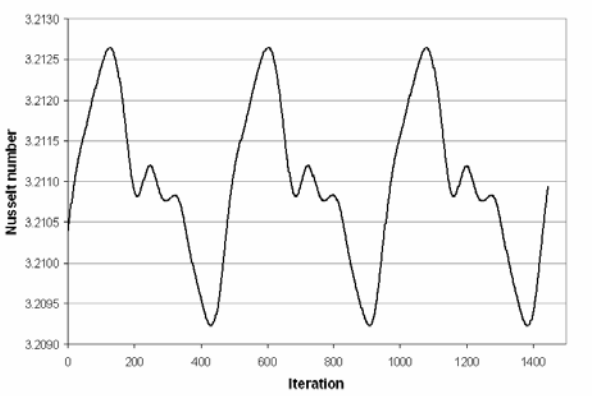


*Figure 2 Typical oscillations in the $Nu_o$ for $Gr=7.5x10^6$, $\theta_o=30^o$ and $\delta_{max}=0.008$*

The small vortex cells in Figure 4 are unstable. They form inside the big cell and move inside the cavity and then merge with the big cell. This behavior causes small oscillations in the Nusselt number, particularly for very high Grashof numbers. In some of the cases, depending on the gap thickness and truncation angle, it is found that the Grashof number of $7.5x10^6$ indicates the transition to turbulent flow.

Figures 5 and 6 show the variation of the Nusselt number ($Nu_o$) as a function of the modified Rayleigh number ($Ra^*$) for truncation angles of 90° and 45°, respectively. The modified Rayleigh number, which was first introduced by Raithby and Hollands [2], is expressed as follows:

$$Ra^* = \frac{Ra\left(\delta_{max}/2\right)}{\left[\left(1+\delta_{max}\right)^{-3/5}+\left(1+\delta_{max}\right)^{4/5}\right]^5} \qquad (15)$$

The figures show that the changes in the Nusselt number as a function of $Ra^{*1/4}$ depend on the non-dimensional gap spacing $\delta_{max}$ for a given truncation angle. This dependence is more significant for the truncation angle of 45°.

Figure 7 shows the effect of the gap thickness on the Nusselt number evaluated at Gr = $5x10^4$, $5x10^5$ and $5x10^6$ for three truncation angles of 90°, 45° and 30°. the figure shows that the Nusselt number increases with the dome truncation angle $\theta_o$. The critical gap thickness that maximizes the heat transfer varies with the truncation angle $\theta_o$, dimensionless gap thickness $\delta_{max}$ and Grashof number. For a truncation angle of $\theta_o$ = 90° the Nusselt number increases with the gap thickness and then converges to an asymptotic value. For truncation angles of $\theta_o$ = 45° and 30° the critical gap thickness increases with the Grashof number.

## CONCLUSION

Natural laminar convection in vertically eccentric domed skylight cavities was investigated when the exterior surface is hotter than the interior one. The control volume approach was used with a commercial CFD package to solve the transient governing equations. The results were obtained for small, moderate and large gap cavities and high and low profile domes ($\theta_o$ = 90°, 45° and 30°) with a wide range of Grashof number ($10^3$ < Gr < $10^7$). For small Grashof numbers, the flow is mono-cellular and reaches the steady state conditions, independently of the gap thickness and truncation angle. For large and moderate Grashof numbers depending on the gap thicknesses and truncation angle, the flow is steady state and may be multi-cellular with one big cell and some small cells inside. The Nusselt number is higher for truncation angle of 90°, and it increases with the dimensionless gap thickness to an asymptotic value. For truncation angels of 45° and 30° the Nusselt number increases with the dimensionless gap thickness and reaches to the maximum value and then decreases. The critical gap thickness that maximizes the heat transfer varies with the truncation angle and Grashof number. The critical gap thickness increases with the Grashof number and gap thickness. For instance at Grashof number of $5x10^6$, the critical gap thickness for $\theta_o$ = 45° and 30° is around $\delta_{max}$ =0.1 and 0.05 respectively. With increasing the Grashof number, small cells appear inside a big cell. These vortex cells become stronger and bigger upon increasing the Grashof number. Depending on the truncation angle and gap thickness, at the Grashof number around $7.5x10^6$ the flow might be unstable and gets into the transition condition to the turbulent regime.

## ACKNOWLEDGEMENTS

This research was funded by NSERC of Canada, the National Research Council of Canada, the Panel for Energy Research and Development (PERD), BC Hydro, and Natural Resources Canada.

## REFERENCES

A. Laouadi and M.R. Atif (2001), Natural Convection Heat Transfer Within Multi-layer Domes, International Journal of Heat and Mass Transfer, Vol. 44, pp. 1973-1981

G.D. Raithby and K.G.T. Hollands (1998), 'Chapter 4, Natural Convection', in Hand book of heat transfer, Editors: W.M. Rohsenow, J.P. Hartnett and Y.I. Cho, McGraw-Hill, New York

V.G. Grag (1991), 'Natural Convection Between Concentric Spheres' International Journal of Heat and Mass Transfer, Vol. 35(8), pp. 1935-1945

H.K. Versteeg and W. Malalasekera (1995), 'An Introduction to Computational Fluid Dynamics the Finite Volume Method', Prentice Hall

FLUENT 6.2 Documentation (2005), Fluent Incorporated, Evanston, Illinois

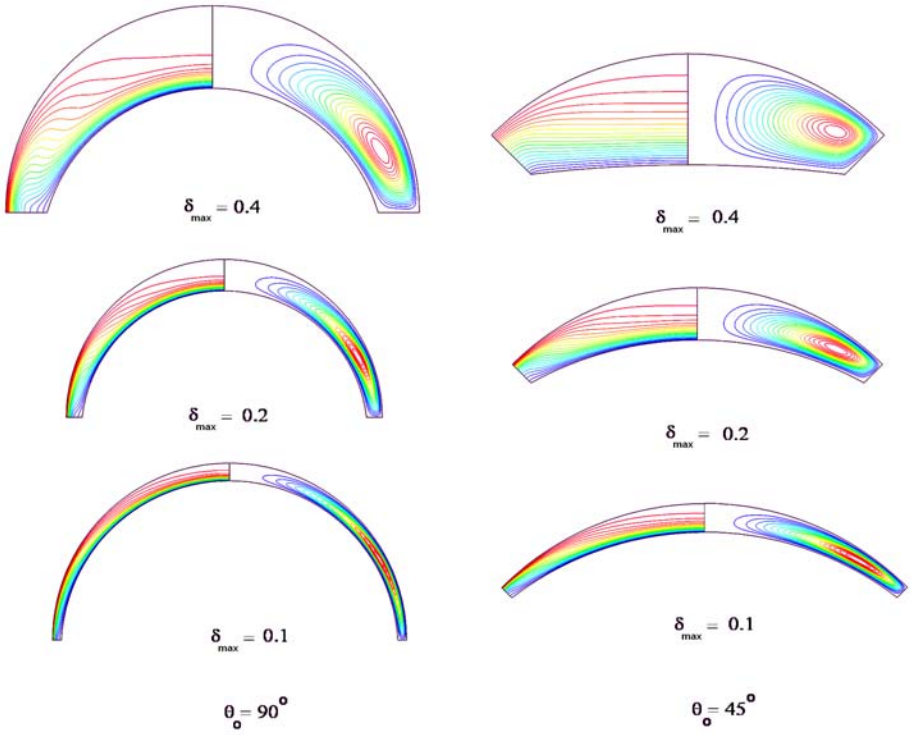


*Figure 3 Streamlines and isotherms for $\theta_o$= 90$^o$ & 45$^o$ and Gr= 5x10$^4$*

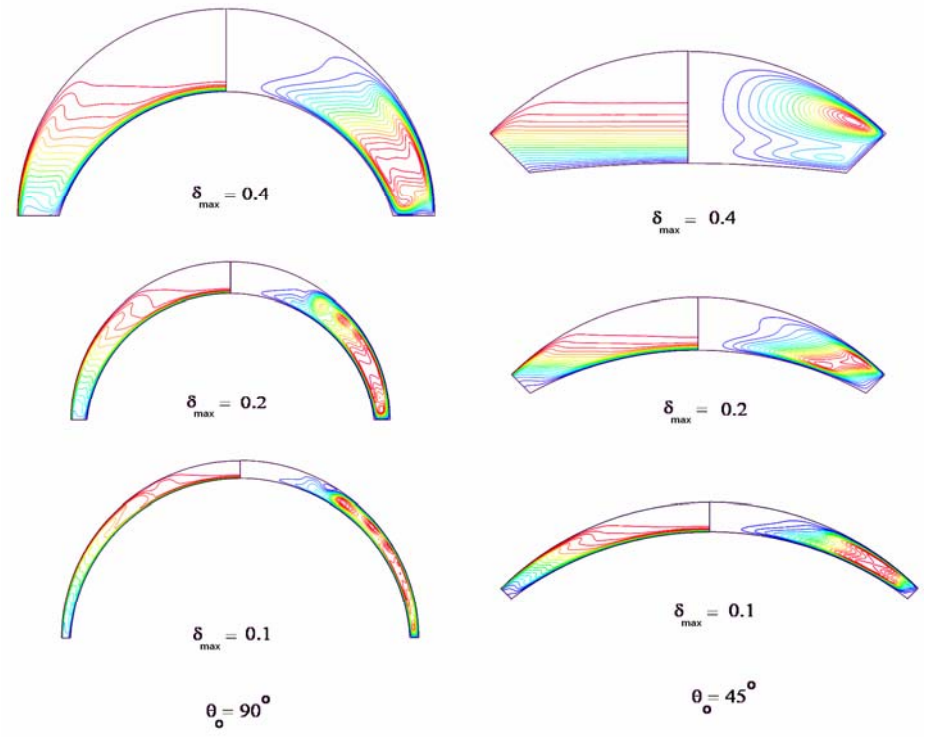


*Figure 4 Streamlines and isotherms for $\theta_o$= 90$^o$ & 45$^o$ and Gr= 5x10$^6$*

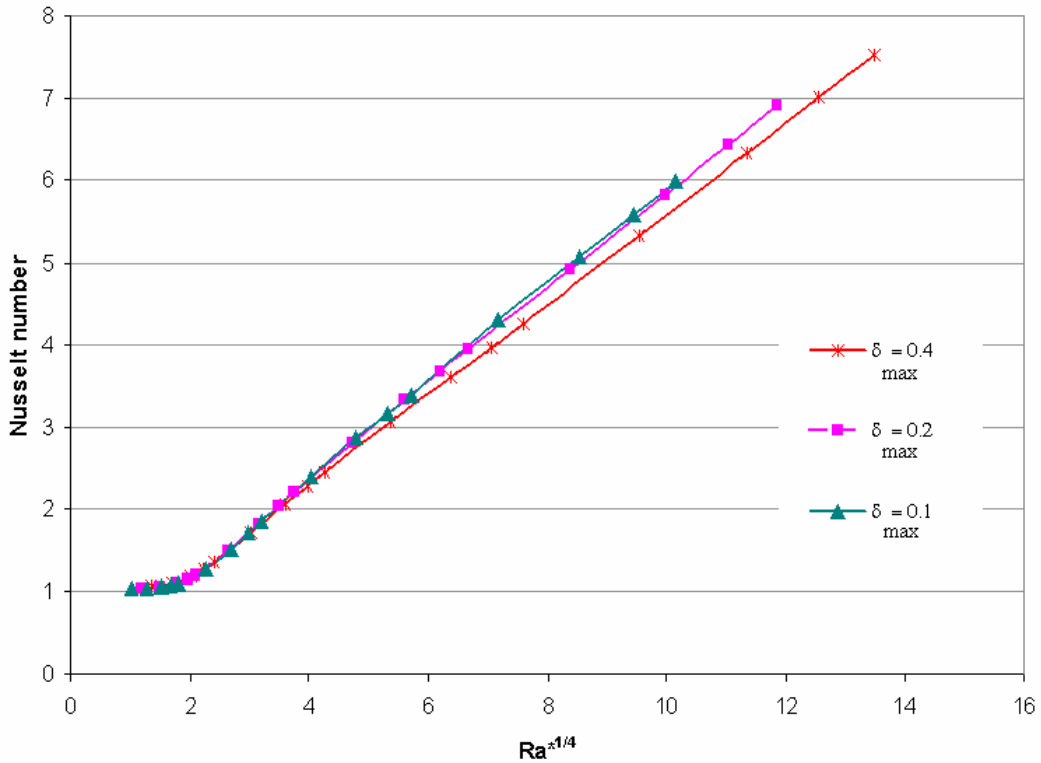


*Figure 5 Profiles of the Nusselt number as a function of $Ra^{*1/4}$ for a truncation angle of 90°*

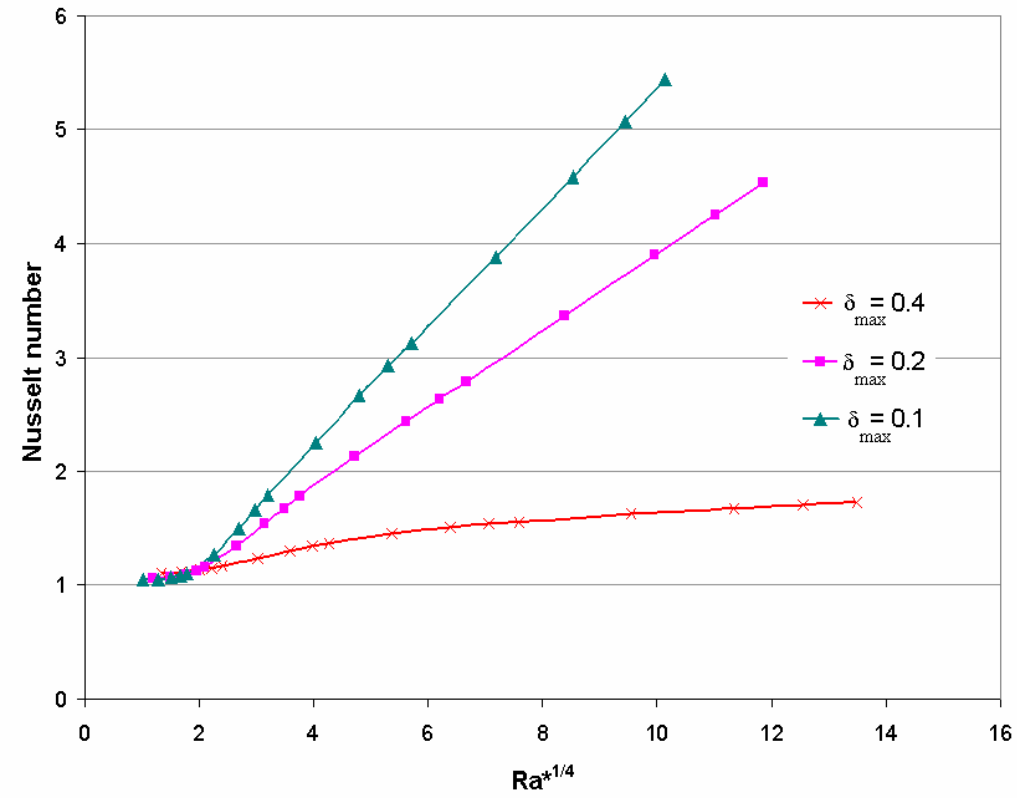


*Figure 6 Profiles of the Nusselt number as a function of $Ra^{*1/4}$ for a truncation angle of 45°*

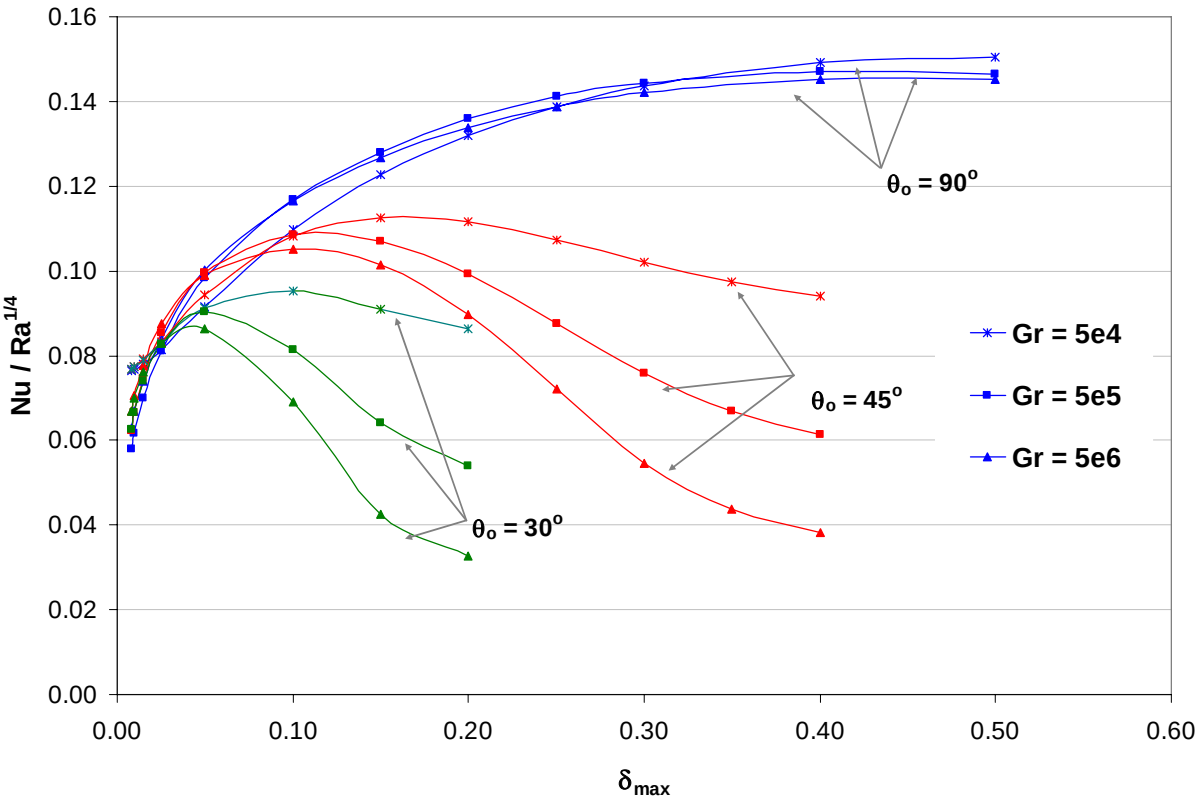


*Figure 7 Profiles of the Nusselt number as a function of* $Ra^{*1/4}$ *and gap thickness* $\delta_{max}$.